

CLIMATE CHANGE

Sustained climate warming drives declining marine biological productivity

J. Keith Moore,^{1*} Weiwei Fu,^{1*} Francois Primeau,¹ Gregory L. Britten,¹ Keith Lindsay,² Matthew Long,² Scott C. Doney,³ Natalie Mahowald,⁴ Forrest Hoffman,⁵ James T. Randerson¹

Climate change projections to the year 2100 may miss physical-biogeochemical feedbacks that emerge later from the cumulative effects of climate warming. In a coupled climate simulation to the year 2300, the westerly winds strengthen and shift poleward, surface waters warm, and sea ice disappears, leading to intense nutrient trapping in the Southern Ocean. The trapping drives a global-scale nutrient redistribution, with net transfer to the deep ocean. Ensuing surface nutrient reductions north of 30°S drive steady declines in primary production and carbon export (decreases of 24 and 41%, respectively, by 2300). Potential fishery yields, constrained by lower-trophic-level productivity, decrease by more than 20% globally and by nearly 60% in the North Atlantic. Continued high levels of greenhouse gas emissions could suppress marine biological productivity for a millennium.

The Southern Ocean strongly influences Earth's climate and biogeochemistry (1, 2). Deep ocean waters upwell to the surface at the Antarctic Divergence. Subantarctic Mode and Antarctic Intermediate waters form as northward-drifting surface waters sink and continue northward at mid-depths, transporting nutrients into the low-latitude thermocline. The Southern Ocean increasingly dominates ocean uptake of heat and CO₂ with strong climate warming because of a poleward shift and intensification of the mid-latitude westerly winds (3–5). Earth system models (ESMs) in the fifth phase of the Coupled Model Intercomparison Project (CMIP5) show consistent declines in global marine net primary production (NPP) during the 21st century in scenarios with high fossil fuel emissions, often with increasing Southern Ocean NPP (4, 6–8).

Biological export of organic matter transfers nutrients vertically as sinking particles decompose, releasing nutrients. Where surface currents diverge (and subsurface currents converge), nutrients are transported upward, but some of the nutrients subsequently rain down as a result of biological export, instead of being advected away laterally at the surface. If the time scale for downward transfer by sinking particles is fast relative to the flushing time, nutrients become trapped, increasing concentrations locally and reducing lateral transport of nutrients out of the area. Idealized model studies, with imposed

increases in Southern Ocean productivity, can develop nutrient trapping that boosts Southern Ocean nutrient concentrations and decreases northward lateral nutrient transport, reducing subsurface nutrient concentrations and decreasing biological productivity at low latitudes (9–16). Southern Ocean nutrient trapping, modulated by circulation, can potentially transfer nutrients from the upper ocean to the deep ocean (12, 15).

We found intense Southern Ocean nutrient trapping as a result of climate warming in a fully coupled simulation to the year 2300, with the Community Earth System Model forced with representative concentration pathway 8.5 (RCP8.5) and extended concentration pathway 8.5 scenarios. The prescribed atmospheric CO₂ concentrations increase to 1960 parts per million by 2250, before leveling off (17, 18). We previously used this ESM to examine marine biogeochemistry to the year 2100 (19–21) and century-by-century changes in the climate-carbon feedback to 2300 (22). Southern Ocean nutrient trapping has not been simulated previously without imposed NPP increases (arbitrarily modifying biological or physical forcings). In our simulation, nutrient trapping develops naturally after centuries of climate warming. This nutrient trapping drives a global reorganization of nutrient distributions, with a net transfer to the deep ocean, leading to a steady decline in global-scale marine biological productivity. This climate-biogeochemistry interaction amplifies the declines in productivity due to increasing stratification projected previously for the 21st century, and its negative effects on productivity eventually exceed those of increasing stratification (6–8).

The Southern Hemisphere westerly winds strengthen and shift poleward with climate warming, approaching Antarctica by 2300 (Fig. 1 and fig. S1). The Antarctic Divergence upwelling zone also strengthens and shifts poleward (1), ultimately

ly initiating coastal upwelling along Antarctica, in areas with downwelling today (Fig. 1 and figs. S1 and S2). Ocean heat content and stratification increase globally, and deep mixing in the North Atlantic collapses, reducing North Atlantic Deep Water (NADW) formation from 30 to 5 sverdrups by 2200 (1 sverdrup = 10⁶ m³ s⁻¹) (21, 22). Global sea surface temperature and stratification (0 to 500 m) peak by 2200 (22). Deeper down, the ocean is still warming in 2300, increasing stratification between intermediate depths and the deep ocean. Density differences between 500 and 1500 m and between 1000 and 2000 m more than double pre-industrial differences by 2300, with most (>80%) of the change occurring after 2100 (table S1). Vertical exchange with cold, deep waters contributes to a slower warming trend in the Southern Ocean at depth, though surface waters warm considerably (Fig. 1 and fig. S4).

Biological export in the Southern Ocean increases by 2100 but declines at lower latitudes and in the high-latitude North Atlantic (table S1). Both patterns intensify after 2100, leading to nutrient trapping, with subsurface nutrient concentrations near Antarctica increasing substantially by 2300 (Fig. 2, fig. S3, and table S2). Concentrations of macronutrients (phosphate, nitrate, and silicic acid) decrease in the northward-subducting waters, decreasing thermocline concentrations and depressing low-latitude NPP and export (Fig. 2, figs. S3 and S4, and tables S1 to S3). Low-latitude productivity steadily drops as stratification increases and both surface and subsurface nutrient concentrations decline (Fig. 2, fig. S3, and tables S1 and S3). The equatorial upwelling flux of phosphate declines sharply (41%), even though the mean equatorial upwelling rate declines modestly (3%). The sharp drop in nutrient flux is due to the decrease in subsurface nutrients after 2100, driven by reduced lateral transport from the Southern Ocean (Fig. 3, fig. S3, and tables S1 and S3).

The nutrients stripped out of surface waters by enhanced productivity in the Southern Ocean are redistributed through the deep ocean by large-scale circulation (Fig. 4). Nutrient concentrations steadily increase in the Southern Ocean and the global deep ocean after 2100, while declining everywhere to the north, from the surface down to the depth of Antarctic Intermediate Water (~1500 m) (Fig. 4). We found similar global redistribution patterns for nitrate and silicic acid but not for iron (figs. S5 to S7), because iron is removed on time scales too short to permit long-range transport (23, 24) (supplementary materials).

Three distinct processes drive the transfer of nutrients to the deep ocean. First, Southern Ocean nutrient trapping lowers the nutrient flux from the deep ocean to the upper ocean within the northward-subducting Antarctic Intermediate and Subantarctic Mode waters. This is the primary pathway for nutrients to return to the upper ocean (12, 15). Second, increasing stratification globally decreases vertical mixing and exchange between the upper and deep ocean (table S1). Third, reduced vertical mixing and reduced NADW formation (21, 22) decrease the main

¹Department of Earth System Science, University of California, Irvine, CA, USA. ²Climate and Global Dynamics Division, Natural Center for Atmospheric Research, Boulder, CO, USA.

³Department of Environmental Sciences, University of Virginia, Charlottesville, VA, USA. ⁴Department of Earth and Atmospheric Sciences, Cornell University, Ithaca, NY, USA.

⁵Oak Ridge National Laboratory, U.S. Department of Energy, Oak Ridge, TN, USA.

*Corresponding author. Email: jkmoore@uci.edu (J.K.M.); weiweif@uci.edu (W.F.)

source of lower-nutrient waters to the deep ocean (12), driving nutrient declines that are larger in the Atlantic basin and high northern latitudes than in other regions (Fig. 4, figs. S5 to S7, and supplementary materials).

Increasing NPP in the Southern Ocean (south of 60°S) is driven by the poleward shift of the westerlies, warming surface waters, and vanishing sea ice, all of which enhance phytoplankton growth. Initially, the rise in NPP is driven by the shifting westerlies, with upwelling rates increasing to the year 2150 before leveling off (Fig. 3A). Surface stratification intensifies to the year 2300, driven by strong surface warming and decreases in surface salinity (Fig. 3, fig. S3, and table S2). The 6°C warming of polar surface waters increases

maximum phytoplankton growth rates by 52% (table S2 and supplementary materials). The mean surface mixed-layer depth shoals with increasing stratification, declining from 75 m in 1850 to 40 m by 2300 (table S2). Sea ice cover reduces radiation to the contemporary Southern Ocean, but this shielding is weakened considerably by 2300 because the ice-covered area declines by 96% (fig. S9 and tables S1 and S2). Mean light levels in the surface mixed layer increase 245% by 2300 as a consequence of near-complete sea ice loss and shoaling mixed-layer depths (table S2 and supplementary materials).

Iron availability modulates phytoplankton capacity to take advantage of improving light and temperature growth conditions. Subsurface iron

concentrations increase by 34% south of 60°S by 2300, with particularly high subsurface concentrations near Antarctica (table S2 and figs. S7 and S10). Volumetric upwelling rates remain ~25% above preindustrial levels after 2150, and the upwelling phosphate flux follows this temporal pattern, boosted modestly by the nutrient trapping effect (table S2 and supplementary materials). In contrast, the iron upwelling flux continues to rise to the year 2300, increasing 276% relative to preindustrial levels (Fig. 3 and table S2). This large increase is due to the southward shift in the upwelling zone, which entrains more margin-influenced, high-iron waters, further boosting productivity (Fig. 2; figs. S2, S3, and S9 to S12; and supplementary materials).

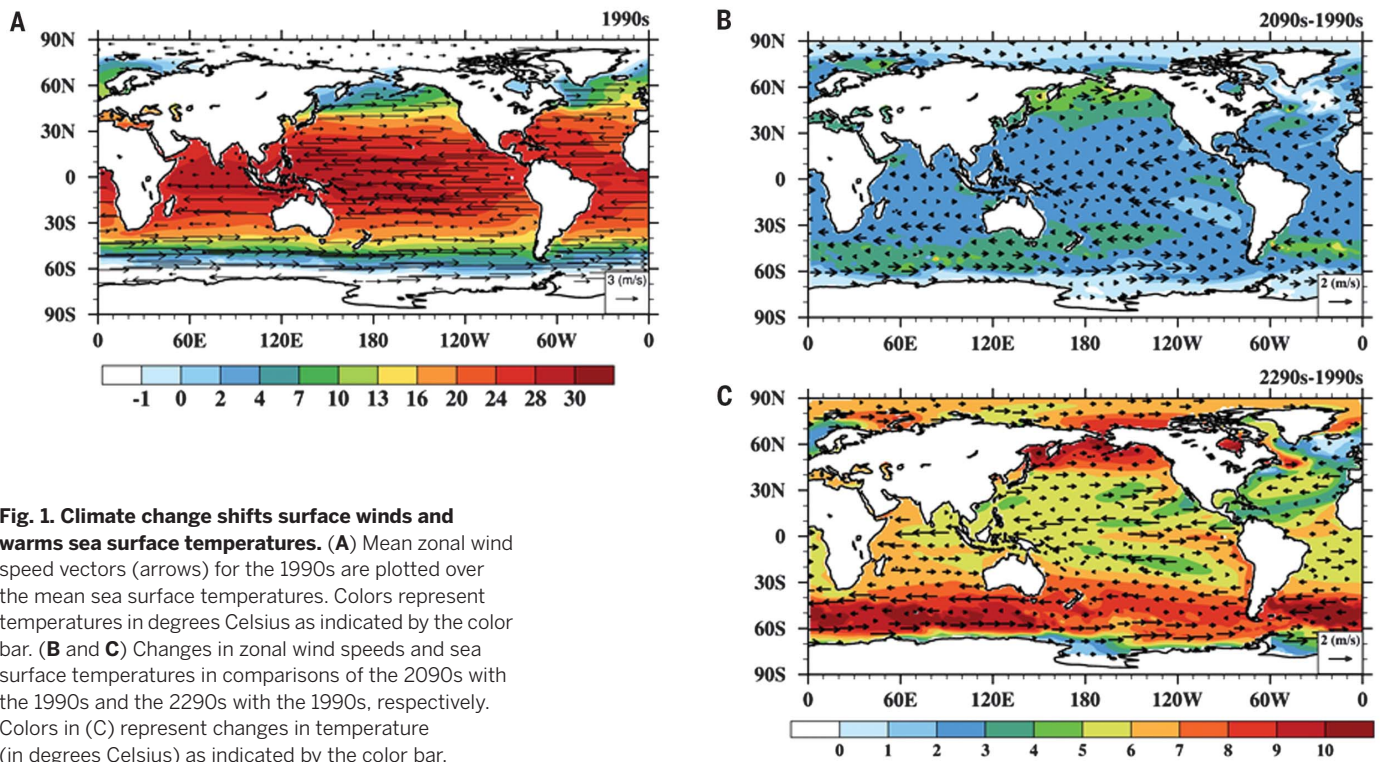
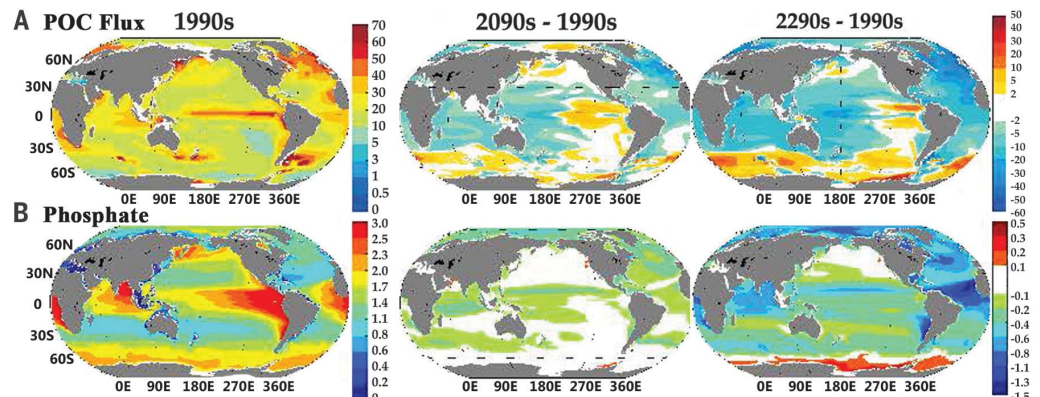


Fig. 1. Climate change shifts surface winds and warms sea surface temperatures. (A) Mean zonal wind speed vectors (arrows) for the 1990s are plotted over the mean sea surface temperatures. Colors represent temperatures in degrees Celsius as indicated by the color bar. (B and C) Changes in zonal wind speeds and sea surface temperatures in comparisons of the 2090s with the 1990s and the 2290s with the 1990s, respectively. Colors in (C) represent changes in temperature (in degrees Celsius) as indicated by the color bar.

Fig. 2. Climate change effects on biological export and nutrient distributions.

Global maps of (A) particulate organic carbon (POC) flux at a depth of 100 m (expressed in grams of carbon per square meter per year) and (B) mean phosphate concentrations at depths of 200 to 1000 m (expressed as micromolar concentrations). The left column shows 1990s means, the middle column shows the difference between the 2090s and the 1990s, and the right column shows the difference between the 2290s and the 1990s. Phosphate concentrations increase around the Antarctic by 2300 because of nutrient trapping.



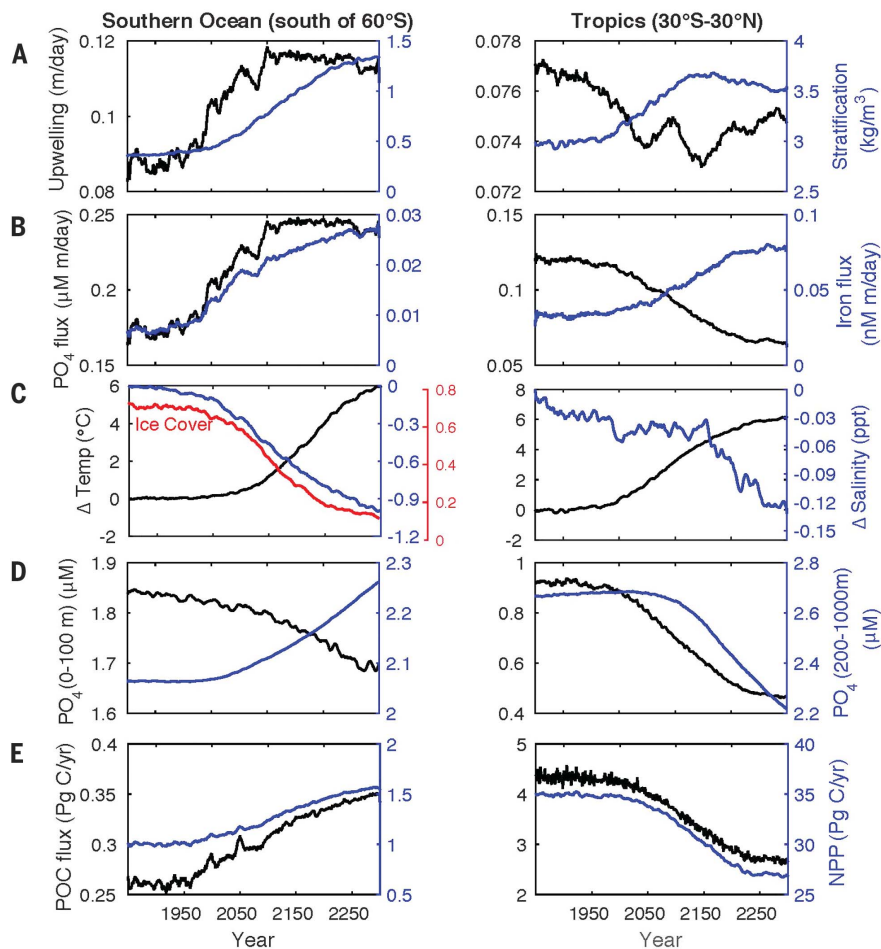


Fig. 3. Regional time series of ocean physical forcing and biogeochemical response.

(A) Evolution of biogeochemical and physical variables over time (1850 to 2300) for the Southern Ocean and the tropics. The mean upwelling rate increases in the Southern Ocean but slows in the tropics, as surface stratification increases in both regions. (B) Upwelling rates for phosphate (expressed as the micromolar concentration per meter of upwelled water per day) and dissolved iron (expressed as the nanomolar concentration per meter of upwelled water per day), (C) changes in temperature and salinity [in parts per thousand (ppt)], (D) surface (0 to 100 m) and intermediate-depth (200 to 1000 m) phosphate concentrations, and (E) sinking POC flux and NPP [both in petagrams of carbon per year (Pg C/yr)]. The fractional sea ice cover is overlain in (C) (left column). Upwelling flux was averaged for 10°S to 10°N for the tropical time series, and stratification was estimated from the density difference between the surface and 200 m for both regions.

Phytoplankton biomass and community composition do not change greatly, but growth rates increase and the growing season is longer, leading to a doubling of the annual biological surface phosphate drawdown by 2300 (table S2). Additional productivity increases are possible with additional iron input, because surface phosphate concentrations are far from depleted. One possible iron source (not included in our simulation) is from Antarctic glaciers (25). The strong climate warming would greatly increase glacial discharge (26), increasing iron inputs, allowing for even more efficient nutrient trapping, and modifying freshwater dynamic forcing of the oceans.

Marine food webs will shift with increasing nutrient stress outside the Southern Ocean. Relative changes in biological export are larger than those in NPP (table S1); because NPP can include sub-

stantial recycled production, changes in export more directly reflect the decreased flux of nutrients to surface waters (8) (tables S1 to S3 and supplementary materials). The smallest phytoplankton benefit most from increasing temperatures and nutrient depletion in surface waters (27), outcompeting larger phytoplankton and reducing the efficiency of biological export (8, 28). Loss of the sea ice biome at both poles will considerably modify biological communities, with reduced competitiveness and, potentially, extinction of some polar-adapted, ice-dependent organisms, including the Antarctic krill central to Southern Ocean food webs (29) (supplementary materials).

Decreasing NPP and biological export north of 30°S more than offset productivity increases in the Southern Ocean, driving global-scale declines

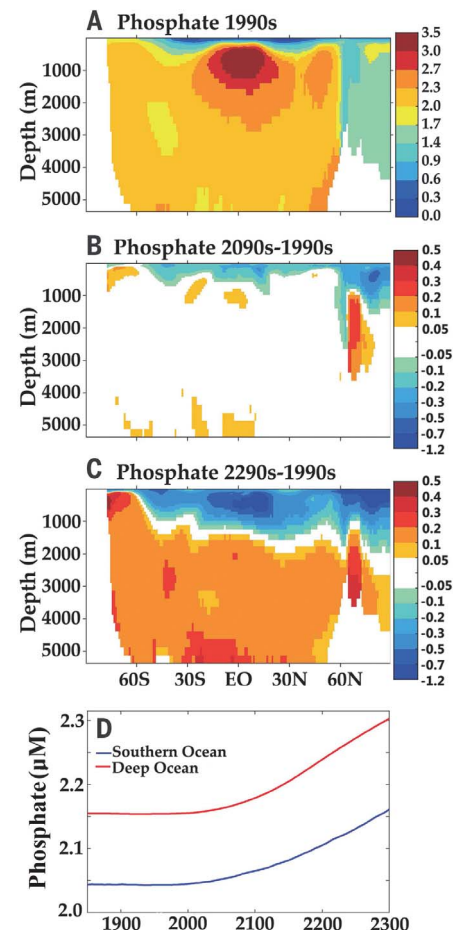


Fig. 4. Southern Ocean nutrient trapping transfers phosphate to the deep ocean. Zonal mean phosphate concentrations (micromolar) are shown for the 1990s (A), along with the differences in zonal phosphate concentrations in comparisons of the 1990s with the 2090s (B) and the 1990s with the 2290s (C). Phosphate concentrations increase over time in the high-latitude Southern Ocean (at all depths south of 60°S) and in the global deep ocean (below 2000 m and north of 60°S) (D).

in NPP (−15%) and export (−30%) by 2300 (figs. S12 and S13 and table S1). The declines above 30°S are 24% for NPP and 41% for particulate organic carbon export (tables S1 to S3). The largest reductions occur in the North Atlantic, western Pacific, and southern Indian oceans, with zooplankton productivity closely tracking phytoplankton (figs. S12 and S13 and tables S1 to S4). Production at higher trophic levels (including potential fishery yield) is limited by lower-trophic-level production and trophic transfer efficiency (30–32). To estimate how changing zooplankton productivity influences higher trophic levels and maximum potential fishery yields, we used an empirical model with optimized transfer efficiencies, constrained by fishery data sets (32) (supplementary materials). We found that for higher trophic levels, production declines by more than

20% globally and by nearly 60% in the North Atlantic (fig. S14 and table S5). Spatial patterns are similar to zooplankton production shifts but are modified by decreasing transfer efficiency where the warm-water biome expands (32) (figs. S13 to S15).

The processes leading to the climate-driven transfer of nutrients to the deep ocean are scarcely apparent by 2100 but dominate ocean biogeochemistry by 2300. Little macronutrient accumulation occurs in the upper ocean around Antarctica by 2100 (Fig. 2 and figs. S3, S5, and S6). This trend is consistent with the finding of only a modest increase in biological carbon storage in the Southern Ocean across multiple CMIP5 models in 2100, driven by a slowdown of the deep circulation rather than by nutrient trapping (4). In 2300, tropical subsurface phosphate concentration is still declining and the deep ocean phosphate level is still increasing linearly (Figs. 3 and 4). Thus, the transfer of nutrients to the deep ocean will continue well past 2300, further depressing upper-ocean nutrient concentrations and global-scale productivity. ESM simulations must extend well past 2100 to capture key ocean physical and biogeochemical responses to multicentury climate warming.

Southern Ocean nutrient trapping appears to be a robust response to multicentury warming. All CMIP5 models project southward shift and intensification of the westerlies over the 21st century under the RCP8.5 scenario, despite considerable differences in the structure and performance of atmospheric models (5). Most CMIP5 models predict increasing Southern Ocean export by 2100, despite large differences in plankton and biogeochemical models (4, 6–8, 24, 28). We found that the same climate-driven nutrient redistribution occurs in two other ESMs [the Hadley Centre Global Environmental Model, version 2 (HadGEM2) (33), and the Max-Planck-Institute Earth System Model (MPI-ESM) (34)] that conducted RCP8.5 simulations to the year 2300 (fig. S16). Both models show nutrient increases in the Southern Ocean and in the deep ocean, accompanied by nutrient reductions in the upper ocean. Thus, our results are not dependent on the model details of atmosphere-ocean circulation, plankton dynamics, or biogeochemistry, but rather seem to represent a robust Earth system response to multicentury climate warming.

Relatively modest increases in export are sufficient to induce nutrient trapping if they occur in the critical location above the Antarctic Divergence. Currently, heavy sea ice cover, cold tem-

peratures, and iron limitation depress biological production in this region. Warming of surface waters and removal of sea ice greatly improve phytoplankton growth conditions, inducing strong regional nutrient trapping that further boosts productivity. If the climate warms enough to remove Southern Ocean sea ice, the nutrient redistribution and depression of global-scale productivity outlined here seem inevitable. Thus, the loss of Southern Ocean sea ice marks a critical biogeochemical tipping point in the Earth system. More research is needed on the physical forcings and the degree of warming necessary for removal of southern sea ice cover and the initiation of Southern Ocean nutrient trapping, including simulations with more moderate future trajectories of fossil fuel emissions. Rapid southern sea ice decline begins in about the year 2050 in our simulation, when mean surface air temperature has risen by ~2.5°C, with near-complete removal of sea ice by 2200 (Fig. 3 and fig. S9). This sea ice trend and the biogeochemical responses documented here support emission reduction targets that keep climate warming below 2°C (26).

The ongoing depletion of upper-ocean nutrients in 2300 will not reverse until the climate cools and sea ice returns to the Southern Ocean, depressing high-latitude productivity and enhancing northward lateral nutrient transfer. Southern Ocean dynamics will dominate this climate-cooling time scale, because the Southern Ocean will dominate ocean uptake of CO₂ by 2300 (figs. S17 and S18 and supplementary materials). The long time scales associated with ocean uptake and storage of anthropogenic CO₂ (35) and the subsequent time necessary for the circulation to return depleted nutrients to the upper ocean (12) ensure that NPP will be depressed for a thousand years or more. This puts the climate change impacts on marine biogeochemistry and productivity on the same time scale as continental ice sheets, with cumulative, catastrophic effects that will be increasingly difficult to avoid with delayed reductions in greenhouse gas emissions (26).

REFERENCES AND NOTES

1. J. L. Russell, K. W. Dixon, A. Gnanadesikan, R. J. Stouffer, J. R. Toggweiler, *J. Clim.* **19**, 6382–6390 (2006).
2. T. L. Frölicher et al., *J. Clim.* **28**, 862–886 (2015).
3. T. Ito et al., *Geophys. Res. Lett.* **42**, 4516–4522 (2015).
4. J. Hauck et al., *Global Biogeochem. Cycles* **29**, 1451–1470 (2015).
5. T. J. Bracegirdle et al., *J. Geophys. Res. Atmos.* **118**, 547–562 (2013).
6. L. Bopp et al., *Biogeosciences* **10**, 6225–6245 (2013).
7. A. Cabré, I. Marinov, S. Leung, *Clim. Dyn.* **45**, 1253–1280 (2015).
8. W. W. Fu, J. T. Randerson, J. K. Moore, *Biogeosciences* **13**, 5151–5170 (2016).

9. J. L. Sarmiento, N. Gruber, M. A. Brzezinski, J. P. Dunne, *Nature* **427**, 56–60 (2004).
10. S. Dutkiewicz, M. Follows, P. Parekh, *Global Biogeochem. Cycles* **19**, (2005).
11. I. Marinov, A. Gnanadesikan, J. R. Toggweiler, J. L. Sarmiento, *Nature* **441**, 964–967 (2006).
12. I. Marinov et al., *Global Biogeochem. Cycles* **22**, GB3007 (2008).
13. A. Oschlies, W. Koeve, W. Rickels, K. Rehdanz, *Biogeosciences* **7**, 4017–4035 (2010).
14. M. Holzer, F. W. Primeau, *J. Geophys. Res. Oceans* **118**, 1775–1796 (2013).
15. F. W. Primeau, M. Holzer, T. DeVries, *J. Geophys. Res. Oceans* **118**, 2547–2564 (2013).
16. B. Bronselaer, L. Zanna, D. R. Munday, J. Lowe, *Global Biogeochem. Cycles* **30**, 844–858 (2016).
17. D. P. van Vuuren et al., *Clim. Change* **109**, 5–31 (2011).
18. Materials and methods are available as supplementary materials.
19. K. Lindsay et al., *J. Clim.* **27**, 8981–9005 (2014).
20. M. C. Long, K. Lindsay, S. Peacock, J. K. Moore, S. C. Doney, *J. Clim.* **26**, 6775–6800 (2013).
21. J. K. Moore, K. Lindsay, S. C. Doney, M. C. Long, K. Misumi, *J. Clim.* **26**, 9291–9312 (2013).
22. J. T. Randerson et al., *Global Biogeochem. Cycles* **29**, 744–759 (2015).
23. J. K. Moore, O. Braucher, *Biogeosciences* **5**, 631–656 (2008).
24. A. Tagliabue et al., *Global Biogeochem. Cycles* **30**, 149–174 (2016).
25. L. J. A. Gerringa et al., *Deep-Sea Res. II* **71**, 16–31 (2012).
26. J. Hansen et al., *PLOS ONE* **8**, e81648 (2013).
27. P. Flombaum et al., *Proc. Natl. Acad. Sci. U.S.A.* **110**, 9824–9829 (2013).
28. C. Laufkötter et al., *Biogeosciences* **13**, 4023–4047 (2016).
29. A. J. Constable et al., *Global Change Biol.* **20**, 3004–3025 (2014).
30. K. M. Brander, *Proc. Natl. Acad. Sci. U.S.A.* **104**, 19709–19714 (2007).
31. K. D. Friedland et al., *PLOS ONE* **7**, e28945 (2012).
32. C. A. Stock et al., *Proc. Natl. Acad. Sci. U.S.A.* **114**, E1441–E1449 (2017).
33. J. Caesar et al., *J. Clim.* **26**, 3275–3284 (2013).
34. M. A. Giorgetta et al., *J. Adv. Model. Earth Syst.* **5**, 572–597 (2013).
35. S. Solomon, G. K. Plattner, R. Knutti, P. Friedlingstein, *Proc. Natl. Acad. Sci. U.S.A.* **106**, 1704–1709 (2009).

ACKNOWLEDGMENTS

We received support from the Reducing Uncertainty in Biogeochemical Interactions through Synthesis and Computation (RUBISCO) Scientific Focus Area (SFA) in the Regional and Global Climate Modeling Program in the Climate and Environmental Sciences Division of the Biological and Environmental Research (BER) Division of the U.S. Department of Energy (DOE) Office of Science (as well as DOE BER Earth System Modeling Program grants ER65358 and DE-SC0016539 to J.K.M. and F.P.). Some authors received additional support from the NSF. The Coupled Model Intercomparison Project received support from the World Climate Research Programme and the DOE Program for Climate Model Diagnosis and Intercomparison. The National Center for Atmospheric Research (NCAR) provided computational and other support. NCAR is sponsored by the NSF.

SUPPLEMENTARY MATERIALS

www.sciencemag.org/content/359/6380/1139/suppl/DC1
Materials and Methods
Supplementary Text
Figs. S1 to S18
Tables S1 to S5
References (36–47)

10 August 2017; accepted 5 February 2018
10.1126/science.aa6379

Sustained climate warming drives declining marine biological productivity

J. Keith Moore, Weiwei Fu, Francois Primeau, Gregory L. Britten, Keith Lindsay, Matthew Long, Scott C. Doney, Natalie Mahowald, Forrest Hoffman and James T. Randerson

Science **359** (6380), 1139-1143.
DOI: 10.1126/science.aao6379

Starving ocean productivity

Projected increases in greenhouse gas emissions could suppress marine biological productivity for a thousand years or more. As the climate warms, westerly winds in the Southern Hemisphere will strengthen and shift poleward, surface waters will warm, and sea ice will disappear. Moore *et al.* suggest that one effect of these changes will be a dramatic decrease in marine biological productivity (see the Perspective by Laufkötter and Gruber). This decrease will result from a global-scale redistribution of nutrients, with a net transfer to the deep ocean. By 2300, this could drive declines in fisheries yields by more than 20% globally and by nearly 60% in the North Atlantic.

Science, this issue p. 1139; see also p. 1103

ARTICLE TOOLS

<http://science.sciencemag.org/content/359/6380/1139>

SUPPLEMENTARY MATERIALS

<http://science.sciencemag.org/content/suppl/2018/03/07/359.6380.1139.DC1>

RELATED CONTENT

<http://science.sciencemag.org/content/sci/359/6380/1103.full>

REFERENCES

This article cites 46 articles, 5 of which you can access for free
<http://science.sciencemag.org/content/359/6380/1139#BIBL>

PERMISSIONS

<http://www.sciencemag.org/help/reprints-and-permissions>

Use of this article is subject to the [Terms of Service](#)